# Weakly interacting spinor Bose–Einstein condensates with three-dimensional spin–orbit coupling*

Shu-Wei Song(宋淑伟)[1,2,3,†], Rui Sun(孙蕊)[1,2,3], Hong Zhao(赵洪)[1,2,3], Xuan Wang(王暄)[1,2,3], and Bao-Zhong Han(韩宝忠)[1,2,3]

[1] State Key Laboratory Breeding Base of Dielectrics Engineering, Harbin University of Science and Technology, Harbin 150080, China
[2] Key Laboratory of Engineering Dielectrics and Its Application, Ministry of Education, Harbin University of Science and Technology, Harbin 150080, China
[3] College of Electrical and Electronic Engineering, Harbin University of Science and Technology, Harbin 150080, China

(Received 6 November 2015; revised manuscript received 16 December 2015; published online 20 February 2016)

Starting from the Hamiltonian of the second quantization form, the weakly interacting Bose–Einstein condensate with spin–orbit coupling of Weyl type is investigated. It is found that the $SU(2)$ nonsymmetric term, i.e., the spin-dependent interaction, can lift the degeneracy of the ground states with respect to the $z$ component of the total angular momentum $J_z$, casting the ground condensate state into a configuration of zero $J_z$. This ground state density profile can also be affirmed by minimizing the full Gross–Pitaevskii energy functional. The spin texture of the zero $J_z$ state indicates that it is a knot structure, whose fundamental group is $\pi_3(M) \cong \pi_3(S^2) = Z$.

**Keywords:** Bose–Einstein condensate, spin–orbit coupling, knot

**PACS:** 03.75.Lm, 03.75.Mn, 67.85.Fg, 67.85.Jk **DOI:** 10.1088/1674-1056/25/4/040305

## 1. Introduction

It is well known that the Bose–Einstein condensate (BEC) supplies us with nearly an ideal platform to investigate quantum phenomena with the help of lasers and magnetic fields. For example, the interactions between atoms can be manipulated by changing the strength of an applied magnetic or electric field for species that have a Feshbach resonance.

In 2008, Wu *et al.* theoretically explored the isotropic Rashba spin–orbit coupled Bose–Einstein condensation and spin–spiral-type condensate, and a half-quantum vortex was observed.[1] In 2009, artificial external gauge potentials coupled to neutral atoms were generated by controlling atom-light interaction.[2] Due to the presence of the spin–orbit coupling mechanism, the energy spectrum changes dramatically. The single particle energy minimum has finite momentum and the ground states are circularly degenerate, in which case the ground state of the condensate favors mainly the "stripe" or "plane wave" phase.[3–5] Therefore, spin–orbit coupled cold atom systems have attracted intensive attention over the last few years,[6–18] such as the studies on topics of Spin Hall effects,[19] Majorana fermions,[20,21] etc. Xu *et al.* theoretically investigated the interesting density patterns of the spin–orbit coupled spinor condensate in the presence of rotation.[22–24] It was found that the condensate may become self-trapped as a result of the spin–orbit coupling and the nonlinearity, resembling the so-called chiral confinement.[25] Zhang *et al.* found that the condensate with spin–orbit coupling exhibited dynamical oscillations similar to the Zitterbewegung oscillation.[26] Deng *et al.* also investigated the spin–orbit coupled condensate in the presence of the dipole–dipole interactions.[27] For a weakly interacting bosons system, the spin–orbit coupled condensate favors a ground state with a zero or finite $z$ component of the total angular momentum.[28,29]

For the spin–orbit coupled condensate of three dimensions, Anderson and Clark investigated the single-particle characteristics and found that the system showed a dimensional reduction from three to one and the single-particle spectrum could be well approximated by Landau levels in the radial coordinate and the splittings were inversely proportional to the spin–orbit coupling strength. Kawakami *et al.* found that the three-dimensional skyrmion appeared as the ground state of $SU(2)$ symmetric BECs coupled with a non-Abelian gauge field.[30] Li *et al.* found that the topology of condensate wavefunctions manifested in the quaternionic representation.[31] The spatial distributions of the quaternionic phase show three-dimensional skyrmion configurations, and non-zero Hopf invariants of topological objects in $S^2$ spin orientation was also observed. Recently, Liu and Yang from Beijing Normal University observed the novel topological object three-dimensional dimeron in trapped two-component BECs and explored both exact static and moving solitonic solutions in $F = 1$ BECs.[32,33] However, the $SU(2)$ nonsymmetric BEC with three-dimensional spin–orbit coupling of Weyl type has

*Project supported by the National Natural Science Foundation of China (Grant No. 11447178).
†Corresponding author. E-mail: japical@live.cn
© 2016 Chinese Physical Society and IOP Publishing Ltd 

not been definitely investigated as far as we know. Among the factors which would determine the nontrivial ground states, what role does the spin-dependent interaction play?

In the present paper, we investigate the weakly interacting two-component condensate with three-dimensional spin-orbit coupling of Weyl type. It is found that finite spin-dependent interaction drives the condensate into zero total angular momentum ($J_z = 0$) ground state. Numerically minimizing the full Gross–Pitaevskii energy functional, the state with only spin-dependent interaction favors a knot structure, whose topological Hopf charge is $Q_H = 1$. The paper is organized as follows. In Section 2, we show the single-particle energy spectrum and the eignstates as well. In Section 3, the ground state with weak interaction is investigated within the basis vectors obtained in Section 2. In addition, the imaginary time evolution method is also exploited to confirm the numerical results. Finally, a summary is presented in Section 4.

## 2. Single-particle spectrum

We begin with the single-particle Hamiltonian

$$\hat{h}_0 = \hat{\boldsymbol{p}}^2/2m + \lambda\hat{\boldsymbol{p}}\cdot\boldsymbol{\sigma} + m\omega^2 r^2/2,$$

where $\boldsymbol{\sigma}$, $\hat{\boldsymbol{p}}$, and $\lambda$ are the Pauli matrices, the momentum operator, and spin–orbit coupling parameter, respectively. The atom mass and parabolic trapping frequency are $m$ and $\omega$, respectively. Scaled by the parabolic potential, the dimensionless single-particle hamiltonian can be obtained as

$$\hat{h}_0 = -\nabla^2/2 - \mathrm{i}\kappa\nabla\cdot\boldsymbol{\sigma} + r^2/2, \tag{1}$$

where the time, energy, and length are scaled by $1/\omega$, $\hbar\omega$, and $\sqrt{\hbar/m\omega}$, respectively. The dimensionless spin–orbit coupling parameter is $\kappa = \lambda\sqrt{m/\hbar\omega}$.

Because of the spin–orbit coupling, the orbital angular momentum is not conserved any more. The total angular momentum $\boldsymbol{J} = \boldsymbol{L} + \boldsymbol{S}$ ($\boldsymbol{L}$ and $\boldsymbol{S}$ are the orbital angular momentum and spin angular momentum), however, is a conserved quantity since the total angular momentum operator $\hat{\boldsymbol{J}}$ satisfies $[\hat{\boldsymbol{J}}, \hat{h}_0] = 0$. As a result, we can resort to the eigenstates of $\hat{\boldsymbol{J}}^2$ and $\hat{\boldsymbol{J}}_z$ to obtain the single-particle Hamiltonian spectrum in Eq. (1). The eigenstates of $\hat{\boldsymbol{J}}^2$ and $\hat{\boldsymbol{J}}_z$ read[34]

$$|j,m,s\rangle = \begin{pmatrix} C_\uparrow|j+s/2, m-1/2\rangle \\ C_\downarrow|j+s/2, m+1/2\rangle \end{pmatrix}, \tag{2}$$

where

$$C_\uparrow = s\sqrt{\frac{j - sm + (1+s)/2}{2(j+(1+s)/2)}},$$
$$C_\downarrow = -\sqrt{\frac{j + sm + (1+s)2}{2(j+(1+s)/2)}}, \tag{3}$$

where $s = 1$ corresponds to the case that $\boldsymbol{J}$ and $\boldsymbol{S}$ are aligned ($j = l + s$) and $s = -1$ corresponds to the case that they are anti-aligned ($j = l - s$). $|j + s/2, m \pm 1/2\rangle$ denote the eigenstates of the orbital angular momentum operator $\hat{\boldsymbol{L}}_z$ with orbital angular momentum quantum number $j + s/2$ and magnetic quantum number $m \pm 1/2$. The eigenvalues of $\hat{\boldsymbol{J}}^2$ and $\hat{\boldsymbol{J}}_z$ are $j(j+1)\hbar^2$ and $m\hbar$, respectively. As proved in Ref. [34], the single-particle Hamiltonian can be reformed as

$$\hat{h}_0 = \frac{1}{2}\{\mathscr{A}^+, \mathscr{A}^-\} + \kappa\frac{1}{\sqrt{2}}(\mathscr{A}^+ - \mathscr{A}^-), \tag{4}$$

where $\mathscr{A}^+ = \boldsymbol{\sigma}\cdot\hat{\boldsymbol{a}}^\dagger$ and $\mathscr{A}^- = \boldsymbol{\sigma}\cdot\hat{\boldsymbol{a}}$. The operator vectors $\hat{\boldsymbol{a}}^\dagger = (\hat{a}_x^\dagger, \hat{a}_y^\dagger, \hat{a}_z^\dagger)$ and $\hat{\boldsymbol{a}} = (\hat{a}_x, \hat{a}_y, \hat{a}_z)$ are vectors of creation operators and annihilation operators, respectively.

Next, the basis vectors can be constructed by considering the quantum number $n$ in the radial direction,

$$|n,j,m,s\rangle = |n\rangle|j,m,s\rangle = \begin{pmatrix} C_\uparrow|n, j+s/2, m-1/2\rangle \\ C_\downarrow|n, j+s/2, m+1/2\rangle \end{pmatrix}. \tag{5}$$

In the coordinate space, $|n,l,m\rangle$ reads

$$\langle r,\theta,\varphi|n,l,m\rangle = \left[\frac{2^{l+2-n}(2l+2n+1)!!}{\sqrt{\pi}n![(2l+1)!!]^2}\right]^{1/2} r^l\,\mathrm{e}^{-r^2/2}\,\mathrm{F}(-n, l+3/2, r^2)\mathrm{Y}_l^m(\theta,\varphi), \tag{6}$$

where $\mathrm{Y}_l^m$ and F are the spherical harmonic functions and the Kummer confluent hypergeometric function, respectively.

Since both $\hat{\boldsymbol{J}}^2$ and $\hat{\boldsymbol{J}}_z$ commute with the single-particle Hamiltonian, the Hamiltonian can be transformed into block-diagonalization form with respect to quantum numbers $j$ and $m$. After some kind of tedious calculations (see also Ref. [34]), it can be found that

$$\begin{aligned}\langle n',j',m',s'|\hat{h}_0|n,j,m,s\rangle = {} & \mathrm{i}\kappa\delta_{j',j}\delta_{m',m}(\sqrt{n+1}\delta_{n',n+1}\delta_{s',+}\delta_{s,-} - \sqrt{n}\delta_{n',n-1}\delta_{s',-}\delta_{s,+}) \\ & + \mathrm{i}\kappa\delta_{j',j}\delta_{m',m}\sqrt{n+j+1}\delta_{n',n}(\delta_{s',-}\delta_{s,+} - \delta_{s',+}\delta_{s,-}) + (2n+j+1)\delta_{j',j}\delta_{m',m}\delta_{n',n}\delta_{s',s}.\end{aligned} \tag{7}$$

After diagonalizing the Hamiltonian matrix, one can obtain the eigenstates and the corresponding eigenvalues. Figure 1 shows the single-particle spectrum and the density profile of the ground state with quantum numbers $j = 1/2, m = -1/2$. For weak atomic interaction, it is only necessary to consider a finite number of eigenstates at the bottom of the energy spectrum.

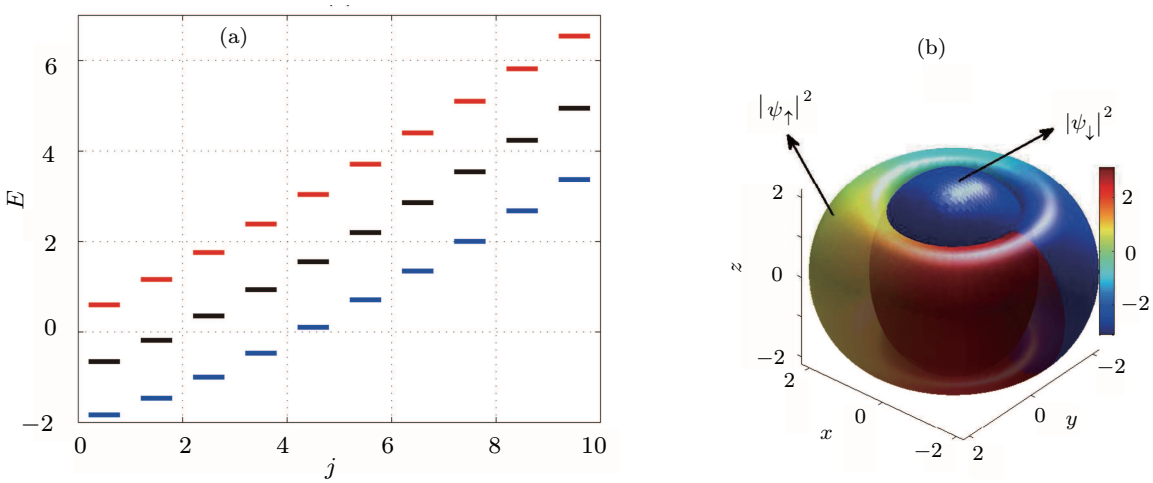



**Fig. 1.** (color online) (a) Single-particle energy spectrum of the three-dimensionally spin-orbit coupled condensate with dimensionless spin–orbit coupling parameter $\kappa = 2$. (b) The isosurface of the density for the single-particle ground state with quantum number $j = 1/2, m = -1/2$ with $|\psi_\uparrow|^2 = 0.002$ and $|\psi_\downarrow|^2 = 0.005$. The color on the isosurface indicates the phase of the state order parameter.

## 3. Spin–orbit coupled condensate with weak interaction

### 3.1. Theoretical model

In the presence of the spin-dependent and spin-independent interactions, the model Hamiltonian in the second quantization form is given by

$$\hat{H} = \hat{H}_0 + \hat{H}_{\rm int}, \tag{8}$$

where

$$\hat{H}_0 = \int {\rm d}\boldsymbol{r} \boldsymbol{\Psi}^\dagger \hat{h}_0 \boldsymbol{\Psi}, \tag{9}$$

$$\hat{H}_{\rm int} = \int {\rm d}\boldsymbol{r} \Big[ \frac{c_0}{2} \psi_a^\dagger \psi_{a'}^\dagger \psi_{a'} \psi_a + \frac{c_1}{2} \psi_a^\dagger \psi_{a'}^\dagger \sigma_{ab}^z \cdot \sigma_{a'b'}^z \psi_{b'} \psi_b \Big]. \tag{10}$$

$\boldsymbol{\Psi} = (\psi_\uparrow, \psi_\downarrow)^{\rm T}$ (the superscript T stands for the transpose) denotes collectively the spinor field operators. $c_0$ and $c_1$ are spin-independent and spin-dependent interaction parameters, and in terms of the effective interaction between different species, they read $c_0 = (g_1 + g_{12})/2$ and $c_1 = (g_1 - g_{12})/2$. In $\hat{H}_{\rm int}$, the Einstein summation convention is used $(a, a' = \uparrow, \downarrow)$.

For a weakly interacting $N$-boson system, only several lowest energy levels are occupied. Thus, the field operator can be expanded as $\Psi = \sum_f \Psi_f \hat{a}_f$, where $\Psi_f$ denotes the single-particle state in Eq. (6), and $\hat{a}_f$ is the corresponding annihilation operator. The many-body Hamiltonian can be rewritten in the second quantization form as

$$\hat{H} = \sum_f \varepsilon_f \hat{a}_f^\dagger \hat{a}_f + \sum_{i,j,k,l} (U_{ijkl} + V_{ijkl}) \hat{a}_i^\dagger \hat{a}_j^\dagger \hat{a}_k \hat{a}_l, \tag{11}$$

where

$$U_{ijkl} = \frac{1}{2} c_0 \sum_{p,q} \int {\rm d}\boldsymbol{r} (\psi_p^i)^* (\psi_q^j)^* (\psi_q^k)(\psi_p^l), \tag{12}$$

$$V_{ijkl} = \frac{1}{2} c_1 \sum_{p,q,r,s} \int {\rm d}\boldsymbol{r} (\psi_p^i)^* (\psi_q^j)^* \boldsymbol{S}_{pr} \cdot \boldsymbol{S}_{qs} (\psi_s^k)(\psi_r^l), \tag{13}$$

and $\varepsilon_f$ is the single-particle energy shown in Fig. 1(a). In $U_{ijkl}$ and $V_{ijkl}$, the summation subscript parameters have values $p, q, r, s = \uparrow, \downarrow$. The many-body Hamiltonian can be solved numerically by using exact diagonalization in the Fock space. The numerical results from the exact diagonalization are also confirmed within the mean-field frame. In the mean-field frame, the operators $\hat{a}_f$ are replaced by complex numbers, and the mean-field energies are minimized under the constraint of total particle number $N$.[29]

### 3.2. $J_z = 0$ state with finite spin-dependent interaction

According to the single-particle spectrum in Fig. 1, it is sufficient to consider eigenstates with $j = 1/2$ and $j = 3/2$ for weak interaction with $c_0(c_1) < 0.001$ and $N < 100$.[28]

In the absence of the spin-dependent interaction, the ground states with $J_z = 0$ and $J_z \neq 0$ are degenerate. That means the states with $J_z = 0$ and $J_z \neq 0$ have identical total energy. However, in the presence of the spin-dependent interaction, the condensate is cast into a zero $J_z = 0$ state. Figures 2(a) and 2(b) show the density profile and phase distribution of the minus $J_z$ state. For the state with plus $J_z$, the three-dimensional vortex structure appears in another component of the condensate, and both the density and phase profiles are similar to that of the state with minus $J_z$. The density and phase profiles of zero $J_z$ state in the absence of the spin-dependent interaction do not show any visible difference compared with the density and phase characteristics in Figs. 2(c) and 2(d). The color on the isosurface indicates the phase of the order parameter. In the presence of the spin-dependent interaction, the ground state favors $J_z = 0$. The corresponding density and phase profiles are shown in Figs. 2(c) and 2(d).

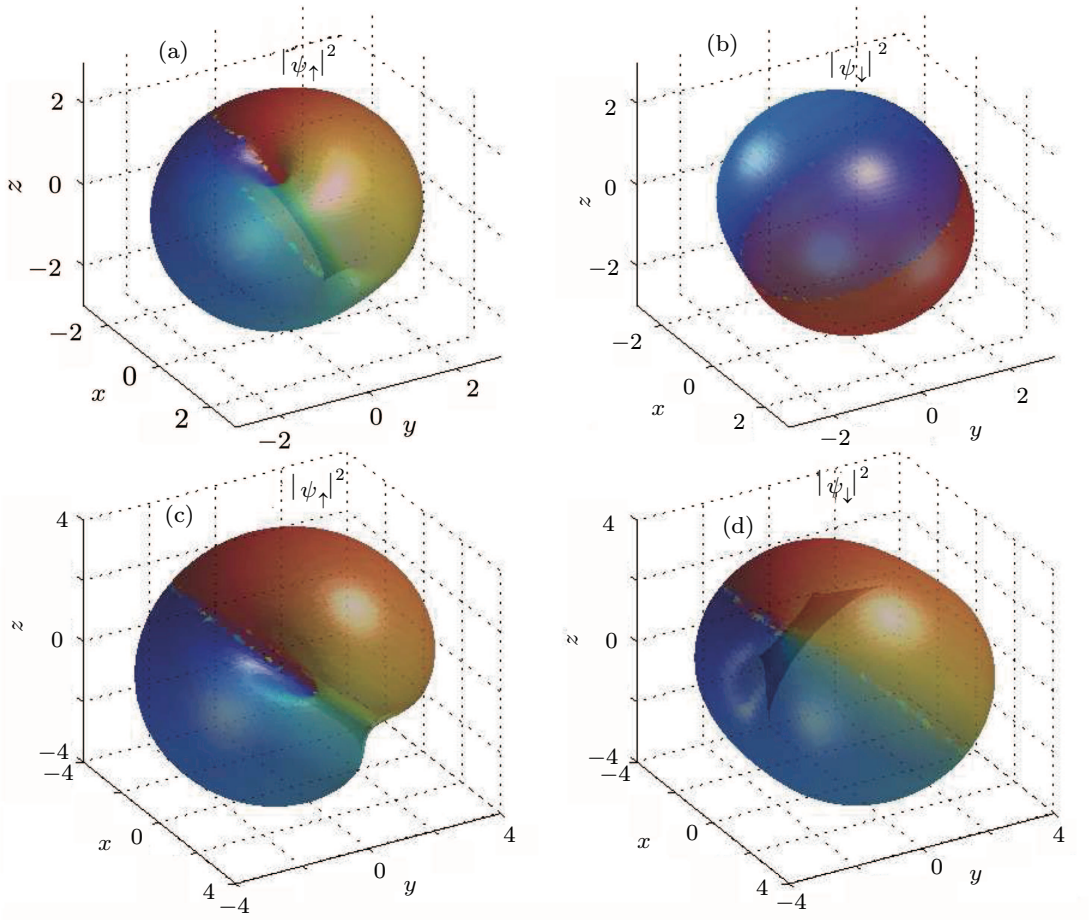



**Fig. 2.** (color online) The density isosurface of $|\psi_\uparrow|^2 = |\psi_\downarrow|^2 = 2\times10^{-4}$. The color on the isosurface indicates the phase of the state order parameter. The state shown in panels (a) and (b) carries $j_z < 0$ with $Nc_1 = 0$, and the state shown in panels (c) and (d) carries $j_z = 0$ with $Nc_1 = 0.001$.

A similar conclusion can also be drawn by minimizing the full Gross–Pitaevskii energy functional realized by promoting the imaginary evolution of the following Gross–Pitaevskii equations[34–37]

$$\begin{aligned}\partial_t\psi_\uparrow &= \left(\frac{1}{2}\nabla^2 - \frac{1}{2}r^2 + \mathrm{i}\kappa\partial_z - g_1|\psi_\uparrow|^2 - g_{12}|\psi_\downarrow|^2 + \mu\right)\psi_\uparrow + \kappa(\mathrm{i}\partial_x + \partial_y)\psi_\downarrow,\\ \partial_t\psi_\downarrow &= \left(\frac{1}{2}\nabla^2 - \frac{1}{2}r^2 - \mathrm{i}\kappa\partial_z - g_{12}|\psi_\uparrow|^2 - g_1|\psi_\downarrow|^2 + \mu\right)\psi_\downarrow + \kappa(i\partial_x - \partial_y)\psi_\uparrow,\end{aligned} \tag{14}$$

where $g_1 = c_0 + c_1$ and $g_{12} = c_0 - c_1$. In the continuous gradient flow equations, the parameter $\mu$ physically corresponds to the chemical potential. These equations are the Gross–Pitaevskii equations for imaginary times and the order parameter $\psi_i$ converges to the stationary state, claiming one of the local minima of the total energy functional. We solve the gradient flow equations from $t$ to $t + \Delta t$ with the two-order Runge–Kutta method.

Figures 3(a) and 3(b) show the sliced three-dimensional density profile with zero $J_z$. The density isosurface profile is the same as that in Fig. 2. By resorting to the spin texture, it is found that such a state is a knotted structure. Knots are topological structures characterized by the third homotopy group and the fundamental group of the order parameter manifold is $\pi_3(M) \cong \pi_3(S^2) = Z$, which can be characterized by a topological invariant called the Hopf charge:[32,38]

$$Q_H = \frac{1}{4\pi^2}\int \varepsilon_{ijk}\mathscr{F}_{ij}\mathscr{A}_k\,\mathrm{d}\vec{r},$$

where $\varepsilon_{ijk}$ is the Levi–Civita symbol and

$$\mathscr{F}_{ij} = \partial_i\mathscr{A}_j - \partial_j\mathscr{A}_i = \boldsymbol{S}\cdot(\partial_i\boldsymbol{S}\times\partial_j\boldsymbol{S}).$$

The pseudospin at the origin and the outmost periphery is $(1,1)/\sqrt{2}$ (the boundary condition). Figure 3(c) shows the preimage of $S_x = 0$ (the torus). The color on the torus denotes the value of $\mathrm{atan}(S_y/S_z)$, indicating the vector orientation on the torus. In Fig. 3(c), we show the preimage for $\boldsymbol{S} = (0,1,0)$ (light green) and $\boldsymbol{S} = (0,0,1)$ (light blue). These two loops interlock once and only once, as illustrated in Fig. 3(d), indicating that $Q_H = 1$.

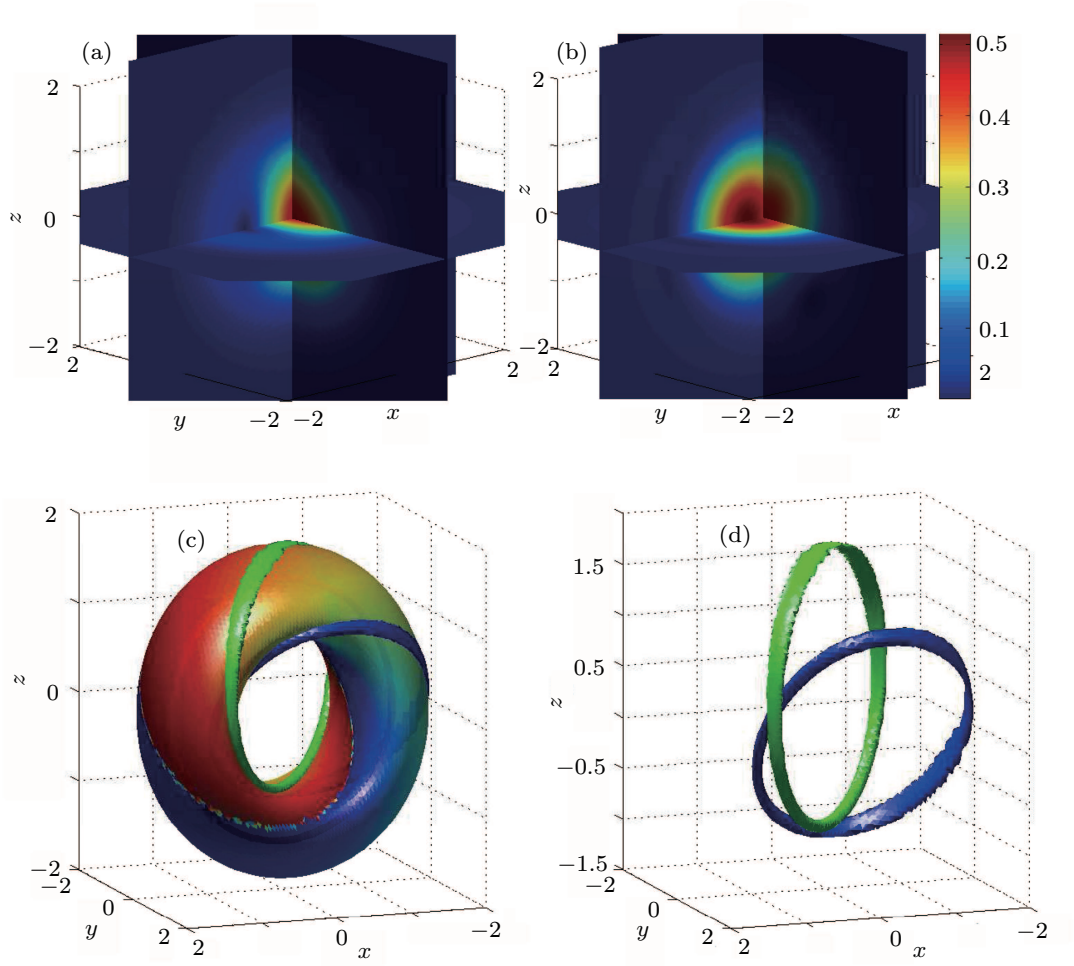



**Fig. 3.** (color online) The sliced three-dimensional density profile of (a) $|\psi_\uparrow|^2$ and (b) $|\psi_\uparrow|^2$ obtained by minimizing the full Gross–Pitaevskii energy functional. The spin–orbit coupling and spin-dependent interaction parameters are $\kappa = 2.0$ and $c_1 = 0.001$, respectively.

## 4. Summary

In summary, we have investigated the weakly interacting two-component BEC with three-dimensional spin–orbit coupling of Weyl type. The role of the $SU(2)$ nonsymmetric term, i.e., the spin-dependent interaction, is clarified. It is found that the finite spin-dependent interaction drives the condensate into $J_z = 0$ ground state. The mean-field numerical results show that the ground state shows a knot spin texture whose topological charge is $Q_H = 1$. This should help us to clarify the effect of the spin-dependent interaction in the process of the cold atom simulation. In addition, the results may shed light on the research of the topological nontrivial objects in cold atom systems.

## References


[1] Wu C J, Ian M S and Zhou X F 2008 arXiv: 0809.3532

[2] Lin Y J, compton R L, Perry A R, Phillips W D, Porto J V and Spielman I B 2009 *Phys. Rev. Lett.* **102** 130401

[3] Zhai H 2012 *Int. J. Mod. Phys. B* **26** 1230001

[4] Zhou X, Li Y, Cai Z and Wu C 2013 *J. Phys. B: At. Mol. Opt. Phys.* **46** 134001

[5] Song S W, Zhang Y C, Wen L and Wang H 2013 *J. Phys. B: At. Mol. Opt. Phys.* **46** 145304

[6] Su S W, Guo S C, Liu I K, *et al.* 2015 *New J. Phys.* **17** 033045

[7] Su S W, Liu I K, Tsai Y C, Liu W M and Gou S C 2012 *Phys. Rev. A* **86** 023601

[8] Aidelsburger M, Atala M, Nascimbene S, Trotzky S, Chen Y A and Bloch I 2011 *Phys. Rev. Lett.* **107** 255301

[9] Fu Z, Wang P, Chai S, Huang L and Zhang J 2011 *Phys. Rev. A* **84** 043609

[10] Campbell D L, Juzeliunas G and Spielman I B 2011 *Phys. Rev. A* **84** 025602

[11] Cheuk L W, Sommer A T, Hadzibabic Z, Yefsah T, Bakr W S and Zwierlein M W 2012 *Phys. Rev. Lett.* **109** 095302

[12] Wang P, Yu Z Q, Fu Z, Miao J, Huang L, Chai S, Zhai H and Zhang J 2012 *Phys. Rev. Lett.* **109** 095301

[13] Zhang Y C, Song S W, Liu C F and Liu W M 2013 *Phys. Rev. A* **87** 023612

[14] Liao R, Huang Z G, Lin X M and Liu W M 2013 *Phys. Rev. A* **87** 043605

[15] Zhu G B, Sun Q, Zhang Y Y, Chan K S, Liu W M and Ji A C 2013 *Phys. Rev. A* **88** 023608

[16] Zhang S S, Yu X L, Ye J and Liu W M 2013 *Phys. Rev. A* **87** 063623

[17] Chen G P 2015 *Acta Phys. Sin.* **64** 030302 (in Chinese)

[18] Bao C G, Xie W F and He Y Z 2015 *Chin. Phys. B* **24** 060305

[19] Beeler M C, Williams R A, Jiménez-García K, LeBlanc L J, Perry A R and Spielman I B 2013 *Nature* **498** 201

[20] Liu X J, Jiang L, Pu H and Hu H 2012 *Phys. Rev. A* **85** 021603

[21] Liu X J and Hu H 2012 *Phys. Rev. A* **85** 033622

[22] Xu X Q and Han J H 2011 *Phys. Rev. Lett.* **107** 200401

[23] Zhou X F, Zhou J and Wu C 2011 *Phys. Rev. A* **84** 063624
[24] Radić J, Sedrakyan T, Spielman I B and Galitski V 2011 *Phys. Rev. A* **84** 063604
[25] Merkl M, Jacob A, Zimmer F E, Ohberg P and Santos L 2010 *Phys. Rev. Lett.* **104** 073603
[26] Zhang Y P, Mao L and Zhang C W 2012 *Phys. Rev. Lett.* **108** 035302
[27] Deng Y, Cheng J, Jing H, Sun C P and Yi S 2012 *Phys. Rev. Lett.* **108** 125301
[28] Hu H, Ramachandhran B, Pu H and Liu X J 2012 *Phys. Rev. Lett.* **108** 010402
[29] Song S W, Zhang Y C, Zhao H, Wang X and Liu W M 2014 *Phys. Rev. A* **89** 063613
[30] Kawakami T, Mizushima T, Nitta M and Machida K 2012 *Phys. Rev. Lett.* **109** 015301
[31] Li Y, Zhou X F and Wu C J 2012 arXiv: 1205.2162
[32] Liu Y K and Yang S J 2015 *Phys. Rev. A* **91** 043616
[33] Liu Y K and Yang S J 2014 *Europhys. Lett.* **108** 30004
[34] Brandon M A and Charles W C 2013 *J. Phys. B: At. Mol. Opt. Phys.* **46** 134003
[35] Bao W, Chern I L and Zhang Y 2013 *J. Comput. Phys.* **253** 189
[36] Bao W and Cai Y 2015 *SIAM J. Appl. Math.* **75** 492
[37] Wang H and Xu Z 2014 *Comput. Phys. Commun.* **185** 2803
[38] Kobayashi M and Nitta M 2013 arXiv: 1304.6021v2